

Supporting Information for

VC₂ and V_{1/2}Mn_{1/2}C₂ nanosheets with robust mechanical, thermal properties as promising materials for Li-ion batteries

Bingwen Zhang^{1,2}, Weiyi Zhang^{1,2}, Qiangqiang Meng³, LeLe Fan³, Qinfang Zhang³

¹*National Laboratory of Solid State Microstructures and Department of Physics,
Nanjing University, Nanjing 210093, China*

²*Collaborative Innovation Center of Advanced Microstructures,
Nanjing University, Nanjing 210093, China and*

³*Key Laboratory for Advanced Technology in Environmental Protection of Jiangsu Province,
Yancheng Institute of Technology, Yancheng 224051, China.*

(Dated: December 14, 2018)

This Supporting Information includes the convergence checks on cut-off energy and Monkhorst-pack k-points, spin-resolved band structures and densities of states of F/O passivated VC₂ and V_{1/2}Mn_{1/2}C₂ nanosheets, optimized adsorption sites for different number of adsorbed Li atoms on (2 × 2) VC₂ and V_{1/2}Mn_{1/2}C₂ nanosheets, and averaged open circuit voltage and specific energy capacity.

I. THE CONVERGENCE CHECKS OF TOTAL ENERGY ON THE CUT-OFF ENERGY AND MONKHORST-PACK K-POINTS

VASP package recommends ENCUT set at 30% larger than ENMAX of POTCAR file. The ENMAX of C, V, and Mn is 273.9 eV, 192.5 eV, and 269.8 eV, respectively, ENCUT=500 eV used in our DFT calculations is thus well above the recommended value. A numerical convergent test of total energy has also been carried out with respect to ENCUT on VC₂ nanosheet and $15 \times 15 \times 1$ Monkhorst-pack k-points set. As shown in Fig. S1(a) below, an energy difference reaches 0.4 meV/atom between 500 eV and 600 eV. Thus, ENCUT=500 eV is a safe choice.

The convergence check of total energy on Monkhorst-pack k-points set $N \times N \times 1$ is done with ENCUT=600 eV. In Fig. S1(b), the total energy is shown as a function of N and converges quickly when N approaches 11. Therefore, $15 \times 15 \times 1$ is large enough for our numerical calculations.

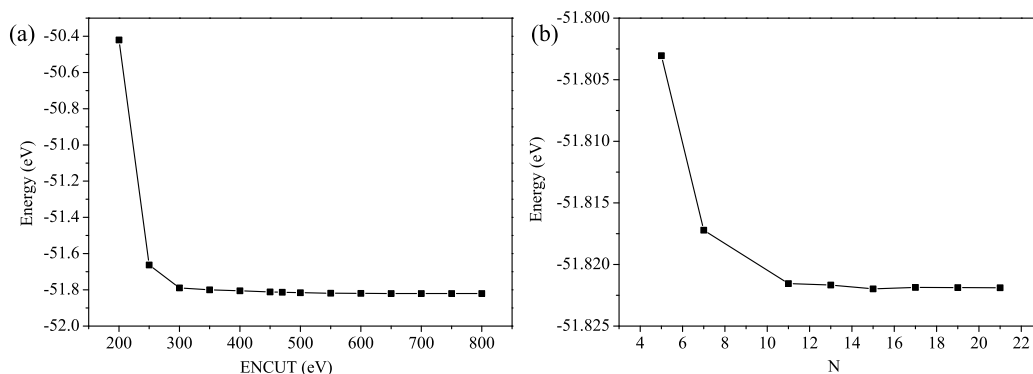


FIG. S1. The convergence check of total energy. (a) With cut-off energy ENCUT; (b) with Monkhorst-pack k-points N .

To check the thermodynamical stabilities of VC₂ and V_{1/2}Mn_{1/2}C₂ nanosheets, we simulated the various bond lengths as functions of time, they are shown in Fig. S2 at 1000K. the deduced standard deviation over average bond-length is around 5% (see Table S1) which showed that these nanosheets are robust against thermal fluctuation.

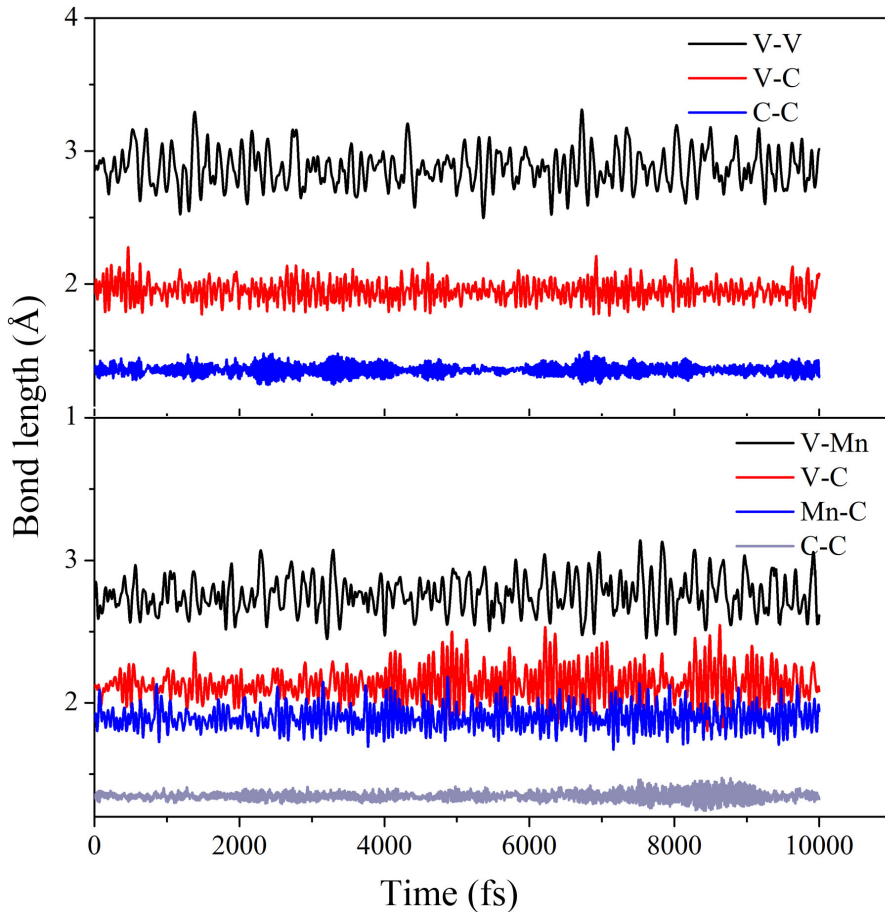


FIG. S2. The various bond-lengths as functions of time.

TABLE S1. The deduced standard deviation (σ/\bar{d}) over average bond-length (V-V, V-Mn, V-C and V-C).

	V-V	V-Mn	V-C	Mn-C	C-C
VC_2	0.041	–	0.035	–	0.026
$\text{V}_{1/2}\text{Mn}_{1/2}\text{C}_2$	–	0.044	0.053	0.043	0.020

II. THE PASSIVATION EFFECT OF O/F ON THE ELECTRONIC AND MAGNETIC STRUCTURES OF VC_2 AND $\text{V}_{1/2}\text{Mn}_{1/2}\text{C}_2$ NANOSHEETS

As listed in Table I of main text, passivation of F/O on VC_2 and $\text{V}_{1/2}\text{Mn}_{1/2}\text{C}_2$ nanosheets can induce ferromagnetic, ferrimagnetic as well as nonmagnetic states. The spin-resolved band structures and densities of states are shown in Supporting Information as Fig. S3 and

Fig. S4 below. It is seen that all passivated states are metallic states irrespective their magnetic properties.

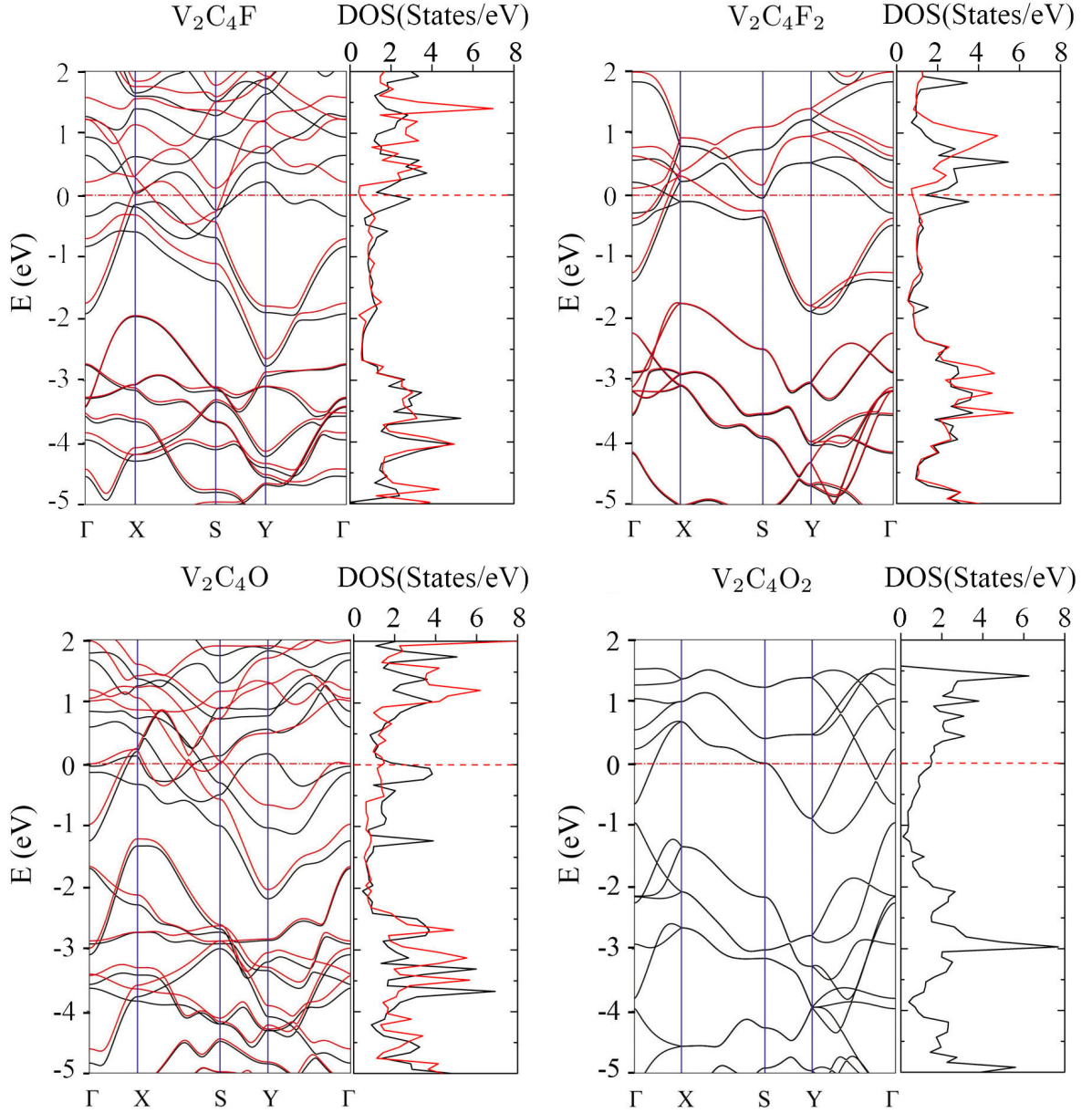


FIG. S3. The spin-resolved band structures and densities of states of O/F passivated VC_2 unit-cell. V_2C_4F , V_2C_4O , $V_2C_4F_2$, and $V_2C_4O_2$ refer to O/F passivations on one side and both sides of nanosheet. The black and red lines refer to the band structures of spin-up and spin-down electrons.

We have also considered one F/O passivated 2×2 supercell. In this case, magnetic structure shown in the Table S2 becomes more complex due to 4 inequivalent Tm sites.

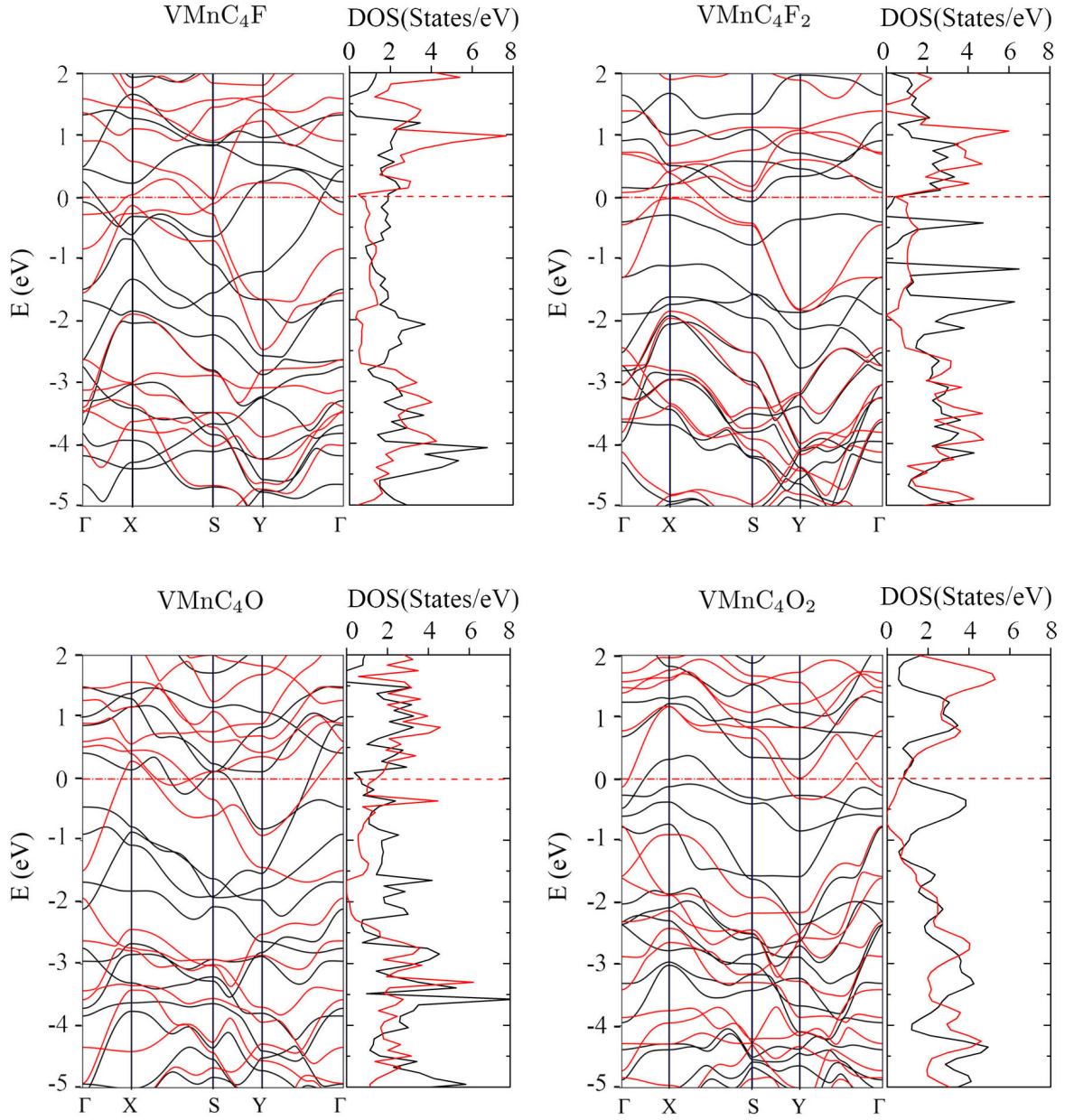


FIG. S4. The spin-resolved band structures and densities of states of O/F passivated $V_{1/2}Mn_{1/2}C_2$ nanosheet. $VMnC_4F$, $VMnC_4O$, $VMnC_4F_2$, and $VMnC_4O_2$ refer to O/F passivations on one side and both sides of nanosheet. The black and red lines refer to the band structures of spin-up and spin-down electrons.

TABLE S2. The magnetic moments (μ/μ_B) and d electrons numbers (nd) of the Tm atoms in 2×2 supercell of $(VC_2)_2$ (VC) and $(V_{1/2}Mn_{1/2}C_2)_2$ (VMnC) after passivation by O/F atom.

	V ₁		V ₂		V ₃ /Mn ₁		V ₄ /Mn ₂	
	μ	nd	μ	nd	μ	nd	μ	nd
VC-F	0.00	3.65	0.00	3.74	0.00	3.77	0.00	3.83
VC-O	0.24	3.69	0.02	3.72	0.00	3.72	0.00	3.86
VMnC-F	-0.36	3.68	-0.21	3.87	1.68	5.12	1.76	5.13
VMnC-O	-0.65	3.69	-0.22	3.83	2.45	5.05	2.51	5.06

III. OPTIMIZED ADSORPTION SITES FOR DIFFERENT NUMBER OF ADSORBED LI ATOMS

In this section, the optimized adsorption sites for different number of adsorbed Li atoms on VC_2 and $V_{1/2}Mn_{1/2}C_2$ nanosheets are presented. The representative cases for $n = 2, 3, 4, 8, 16$ of a $2 \times 2 \times 1$ supercell of VC_2 nanosheet are shown in Fig. S5-S7 with the corresponding Li ion concentration $x = n/8 = 0.25, 0.375, 0.5, 1.0, 2.0$ with respect to the eight most stable adsorbed A1 sites in the supercell. In Fig. S5(a), the four possible combinations of A1 sites for two adsorbed Li ions are presented and their adsorption energies are listed below the configurations. The configuration with an adsorption energy -1.606 eV is the most stable one shown in the main text; Fig. S5(b) illustrates the four possible combinations of A1 sites for three adsorbed Li ions, again the configuration with adsorption energy -1.534 eV has the lowest energy and is presented in the main text; Fig. S6 plots the eight possible combinations of A1 sites for 4 adsorbed Li ions, the configuration with adsorption energy -1.501 eV is the ground state presented in the main text; In the above three cases, one observes that Li ions form a chain-like pattern with nearest neighbor Li ions located in the opposite sides of nanosheet. There is only one combinations of A1 sites for 8 adsorbed Li ions, that is the A1 sites of both sides of nanosheet are all occupied by Li ions. The adsorption energy for this case is -1.268 eV;

For high Li ion concentration $n = 16$ or $x = 2$, all A1-A4 sites have to be considered. There are six different combinations. The configurations and their corresponding adsorption energies are listed in Fig. S7. The configuration with adsorption energy -0.712 eV is the

most stable configuration and presented in the main text. This configuration corresponds to the adsorbed structure that all A1 and A3 sites of VC₂ nanosheet are occupied by 16 Li ions.

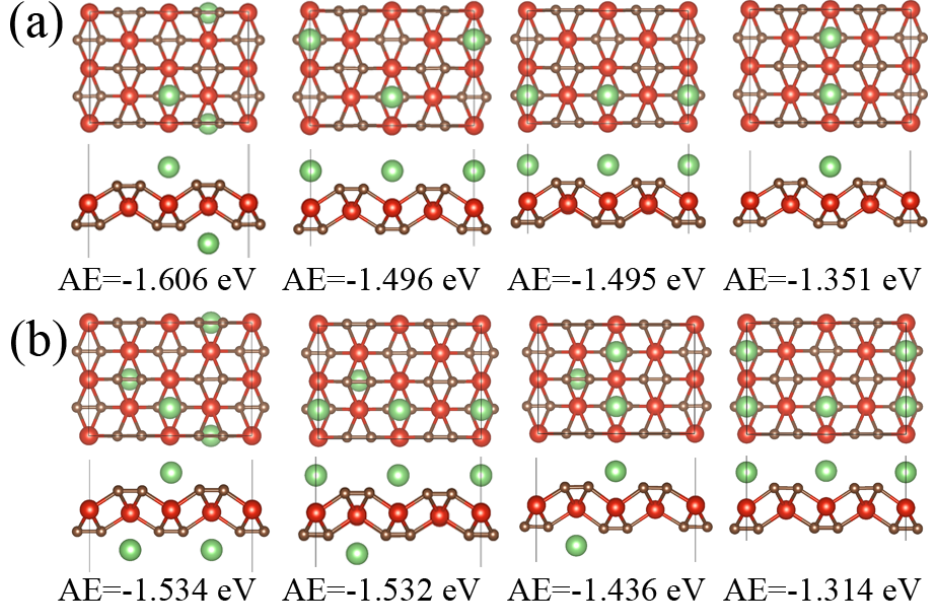


FIG. S5. The configurations and their optimized adsorption energies (eV) for $n = 2, 3$ adsorbed Li ions. (a) $n = 2$, VC₂Li_{0.25}; (b) $n = 3$, VC₂Li_{0.375}.

For V_{1/2}Mn_{1/2}C₂ nanosheet, similar analysis has been carried out to search for the most stable adsorption configuration for different number of adsorbed Li ions. We find the following adsorption rules for a different number of adsorbed Li ions. For $n = 1, 2, 3, 4$, adsorbed Li ions occupy the B5 sites with two Mn above and below and two Vs on the left and right; when $n = 8$, both B5 and B1 of both sides are occupied by Li ions. While for $n = 16$, all B5, B1, B7, and B3 sites are occupied by 16 adsorbed Li ions. The adsorption energies are -1.709 eV ($n = 2$), -1.614 eV ($n = 3$), -1.546 eV ($n = 4$), -1.116 eV ($n = 8$), and -0.644 eV ($n = 16$).

IV. AVERAGED OPEN CIRCUIT VOLTAGE

With the adsorption energies obtained for different number of adsorbed Li ions, averaged open circuit voltage (OCV(x)) and specific energy capacity (J(x)) are defined for VC₂ and

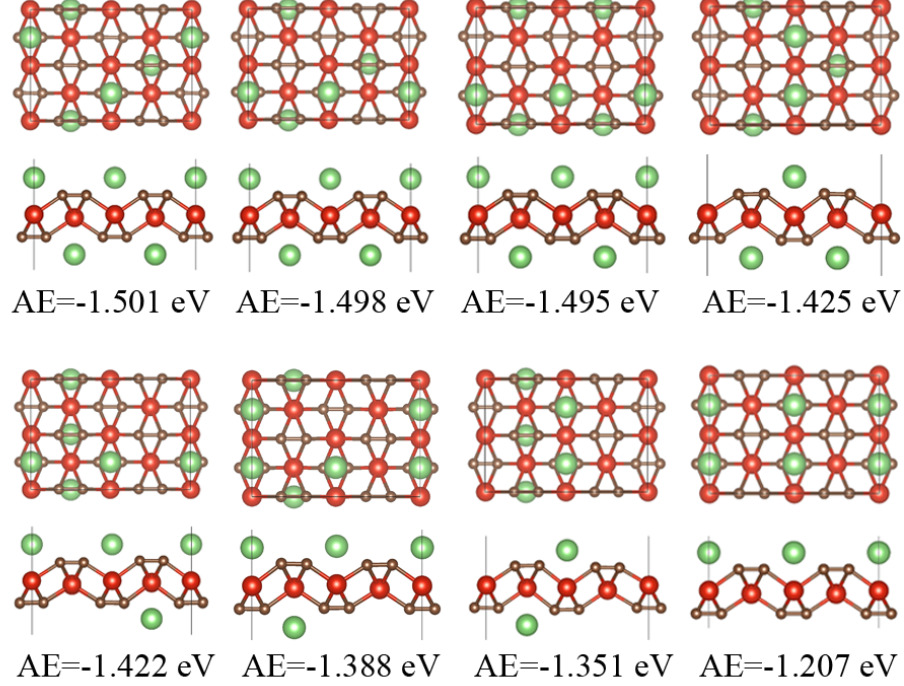


FIG. S6. The configurations and their optimized adsorption energies (eV) for $n = 4$ adsorbed Li ions: $\text{VC}_2\text{Li}_{0.5}$.

$\text{V}_{1/2}\text{Mn}_{1/2}\text{C}_2$ nanosheets at Li ion concentration x by formulae

$$\text{OCV}(x) = \frac{E_{(\text{TmC}_2)} - E_{(\text{TmC}_2\text{Li}_x)} + xE_{\text{Li}}}{x|e|} \quad (1)$$

and

$$J(x) = \frac{Q \times F}{3.6M}. \quad (2)$$

$E_{(\text{TmC}_2)}$, $E_{\text{TmC}_2\text{Li}_x}$, and E_{Li} are the energies per formula unit of TmC_2 , TmC_2Li_x , and Li per atom of bulk body-centered-cubic crystal. $Q = x$ is the charge number per formula unit released during discharge process. $F = 96485.34\text{C/mol}$ is the Faraday constant and M is the atomic mole mass of TmC_2 (g mol^{-1}). $M = 74.96\text{g/mol}$ for VC_2 and 76.96g/mol for $\text{V}_{1/2}\text{Mn}_{1/2}\text{C}_2$. Fig. 6b in main text suggests that Li-ion adsorption process on VC_2 and $\text{V}_{1/2}\text{Mn}_{1/2}\text{C}_2$ nanosheets are stable for $0.25 \leq x \leq 2$. Specific energy capacity are 714.7mAh/g for VC_2 and 696.2mAh/g for $\text{V}_{1/2}\text{Mn}_{1/2}\text{C}_2$ nanosheets if we take $x = 2$.

To better describe the averaged OCV at different charge or discharge stages, one often defines the segmented $\text{OCV}(x_1 = n_1/8, x_2 = n_2/8)$ in Li concentration range $n_1 < n < n_2$

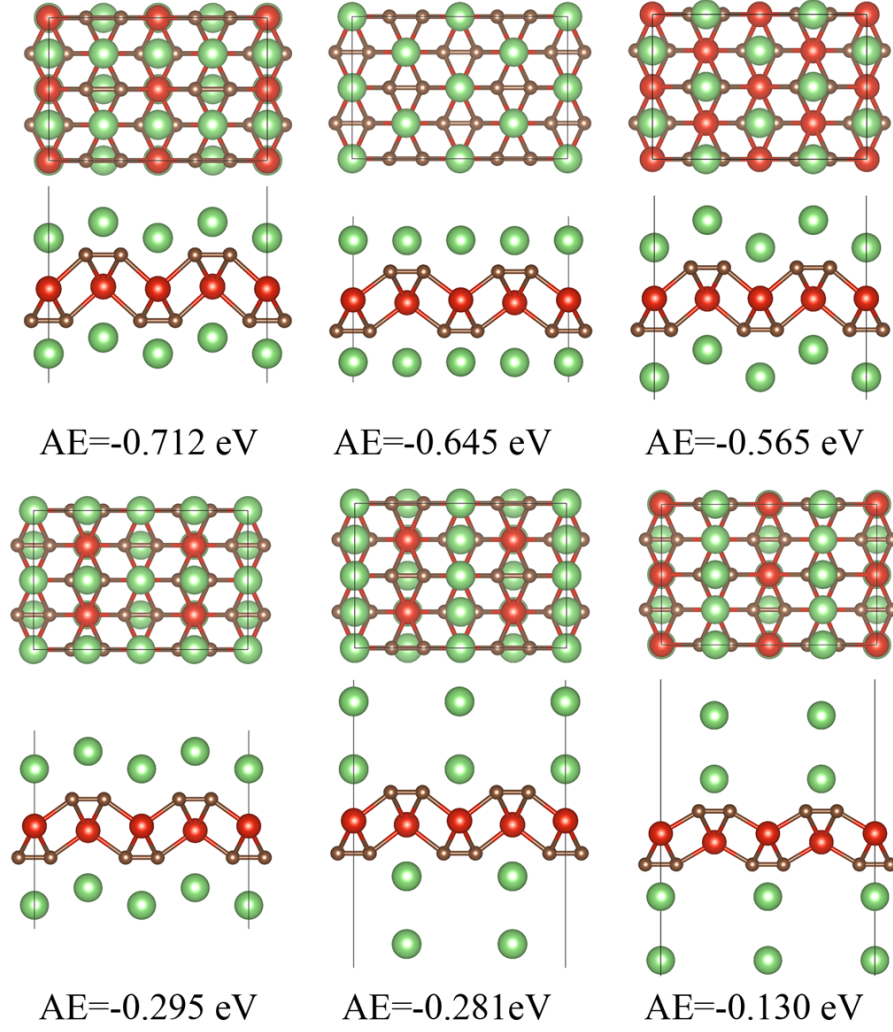


FIG. S7. The configurations and their optimized adsorption energies (eV) for $n = 16$ adsorbed Li ions: VC_2Li_2 .

by

$$OCV(x_1, x_2) = \frac{E_{(TmCLi_{x_1})} - E_{(TmCLi_{x_2})} + (x_2 - x_1)E_{Li}}{(x_2 - x_1)|e|} \quad (3)$$

The averaged OCV calculated using $n_1 = n - 1$ and $n_2 = n + 1$ are presented in Fig. S8b. It is seen that OCV is charge-state dependent and one can use OCV function to optimize the battery charge and discharge process.

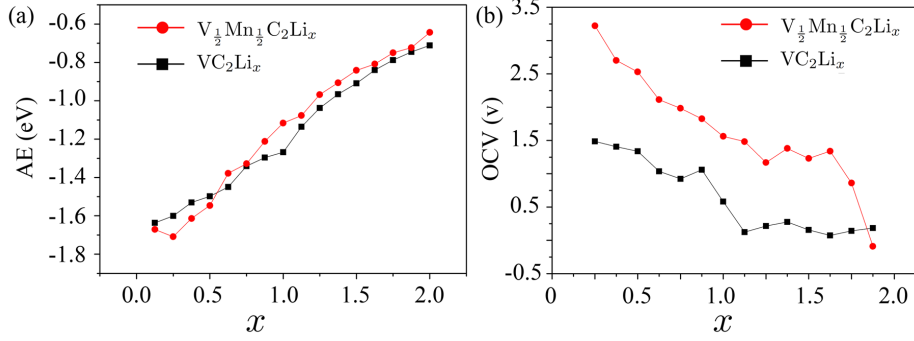


FIG. S8. (a) The adsorption energy per Li atom in TmC_2Li_x ; (b) OCV of TmC_2Li_x versus x .

V. DOUBLE-LAYER STRUCTURE AND VAN DER WAALS INTERACTION CORRECTION

To consider the stacking effect we have also considered double-layer case of TmC_2 . In the absence of van der Waals (vdW) interaction correction, the optimized Tm-Tm distances between the layers are around 5.7Å and 6.1Å for VC_2 and $V_{1/2}Mn_{1/2}C_2$, respectively. The small interlayer space removes half of the Li-ion adsorption sites between the layers, the maximum Li-ion storage capacity is reduced to $(N+1)/2N$ with respect to that of single layer (N is number of layers). As shown in the Fig. S9 below, for the optimized adsorption configurations of 2×2 supercells and at the same Li-ion concentration, the averaged AE is always lower for double-layer than for single layer although the maximum Li-ion storage capacity is reduced by 25% for double-layer.

Using the recommended optB86b-vdW correction, the optimized Tm-Tm distance between the layers are updated to 4.8Å and 5.1Å for VC_2 and $V_{1/2}Mn_{1/2}C_2$, respectively. There are 15.8% and 16.4% reductions for VC_2 and $V_{1/2}Mn_{1/2}C_2$, respectively. As shown in the Fig. S10, including van der Waals interaction correction generally reduces the averaged adsorption energy (AE) because of the stronger binding between the two layers.

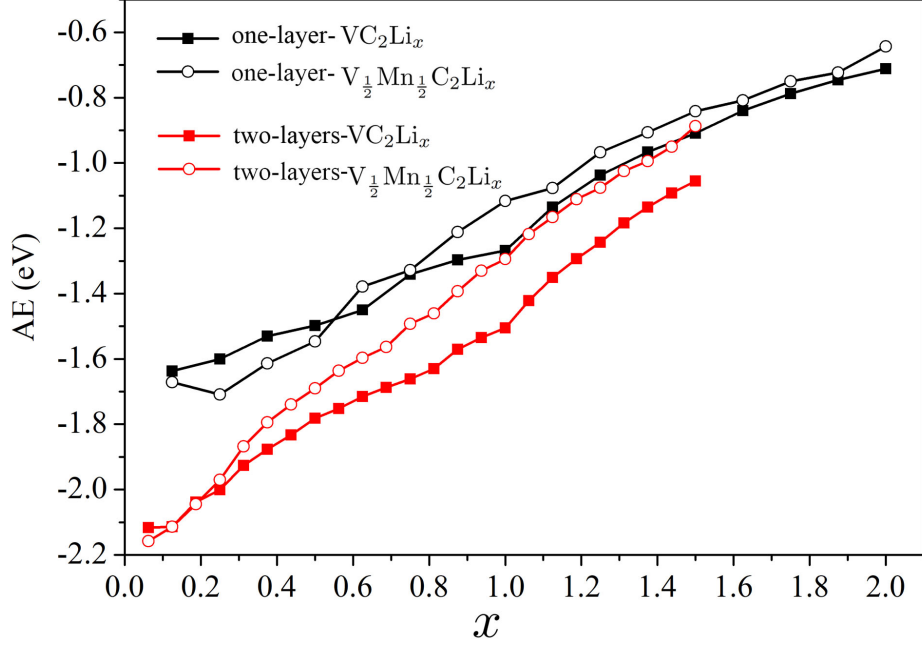


FIG. S9. Dependence of adsorption energy as functions of Li-ion concentration for both single- and double-layer TmC_2 in the absence of vdW interaction correction.

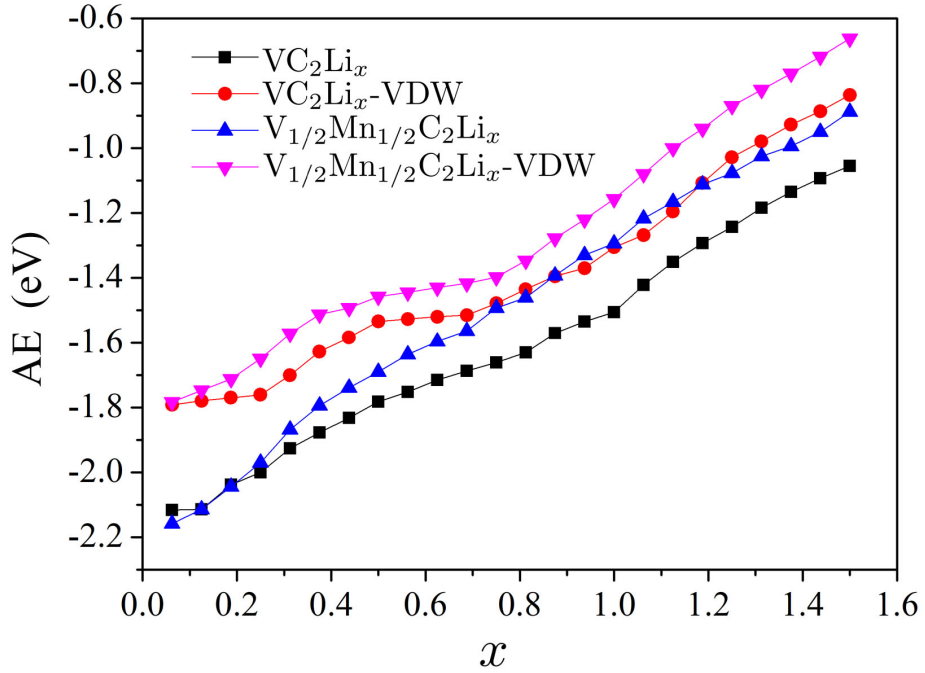


FIG. S10. Dependence of adsorption energy as functions of Li-ion concentration for double-layer TmC_2 with or without vdW interaction correction.